Experimental Neurology 334 (2020) 113435

Contents lists available at ScienceDirect

Experimental Neurology

journal homepage: www.elsevier.com/locate/yexnr

Short Communication

Concussion increases CA1 activity during prolonged inactivity in a familiar environment

Shanti R. Tummala*, Matthew A. Hemphill, Andrea Nam, David F. Meaney*

Department of Bioengineering, School of Engineering and Applied Sciences, University of Pennsylvania, Philadelphia, PA, USA

ARTICLE INFO

Keywords:
TBI
Blast
Miniscope
Novel
Open field
Home cage
CNMF-E
GCamp6f

ABSTRACT

Although hippocampal damage plays a key role in impairments after concussion, differences in hippocampal information processing during recovery are unknown. Micro-endoscopic calcium imaging was performed before and after primary blast injury in freely behaving mice in two environments: their familiar home cage and a novel open field. Results show that after concussion CA1 activity increased in the familiar environment in which animals were awake and mostly immobile but was unaltered in a novel environment which the animals actively and constantly explored. As awake immobility parallels cognitive rest, a common treatment for patients, the results imply that prolonged cognitive rest may unwittingly impede concussion recovery.

The architecture of neural circuits and the coordination of their activity are instrumental for cognitive function. Mechanical impact to the brain (concussion or mild Traumatic Brain Injury; mTBI) disrupts the coordination between neural circuits by damaging their architecture and leads to pronounced changes in cognition that can affect the quality of life for years (Meaney et al., 2014). The circuits of the hippocampal formation involved in learning and memory are among those affected by mTBI (Paterno et al., 2017). However, despite decades of research and numerous in situ studies on the electrophysiological changes occurring in the hippocampal formation (Atkins, 2011), it is unknown how hippocampal circuits respond in vivo after mTBI, especially as the animal explores and processes information about its environment. Here, through calcium imaging in area CA1 of animals behaving freely in their familiar home cages (HC) and a novel open field (OF), we address this knowledge gap and report for the first time that mTBI modifies CA1 activity during prolonged awake immobility in the familiar HC but does not impede the ability to detect contextual novelty in an OF.

Area CA1 is integral for detecting and encoding contextual novelty (Lisman and Otmakhova, 2001). Previous work shows enhanced inhibition and reduced Schaffer collateral evoked field responses in CA1 after mTBI (Beamer et al., 2016; Chen et al., 2018; Johnson et al., 2014; Witgen et al., 2005). To appreciate how this increased inhibition affects CA1 circuits in vivo, we designed a simple experimental paradigm that observed CA1 activity in both familiar and novel environments on two consecutive days prior to mTBI (−2d, −1d) and on the fifth day (5d) after mTBI (see methods, Fig. 1b, Supplementary Fig. 1), at which time point we previously reported reduced Schaffer collateral evoked field responses and deficits in spatial object recognition (Beamer et al., 2016). Pyramidal neurons in CA1 were transfected with the transgene for the calcium sensor GCamp6f (Supplementary Fig. 3a, Supplementary Table 1) and their activity recorded with a commercial miniature head mounted microscope (iNSCOPIX, CA). We modified the original unstable camera base plate design and customized it to move both vertically and horizontally to ensure that the cells were always in focus (Fig. 1a). Regions of interest (ROI) in the calcium images were first identified automatically (Zhou et al., 2018) and those corresponding with distinct cell bodies (neurons) were retained after manual inspection (Supplementary Fig. 2). The total number of active neurons varied across days in each of the animals (Fig. 1c). Although the total number of active cells appeared to increase after mTBI, the difference was not significant ($p = 0.652$, Friedman's one-way repeated measures ANOVA). Of all the neurons active on any given day, we found that about 13% were active in both the HC and OF environments (Fig. 1d). Examining the event rates (Fig. 1e) and amplitudes (Supplementary Fig. 3b) of these cells, we found that mTBI did not alter the correlation in their activity in the two environments. The remaining neurons were uniquely active in either the HC (around 42%) or OF (around 45%). These fractions were similar across all the days and were not altered by injury. However, as images could not be satisfactorily registered across days, we were unable to judge if the active population in each environment was the same on all the days.

* Corresponding authors.
E-mail addresses: stummala@seas.upenn.edu (S.R. Tummala), dmeaney@seas.upenn.edu (D.F. Meaney).

https://doi.org/10.1016/j.expneurol.2020.113435
Received 14 April 2020; Received in revised form 2 August 2020; Accepted 12 August 2020
Available online 17 August 2020
0014-4886/

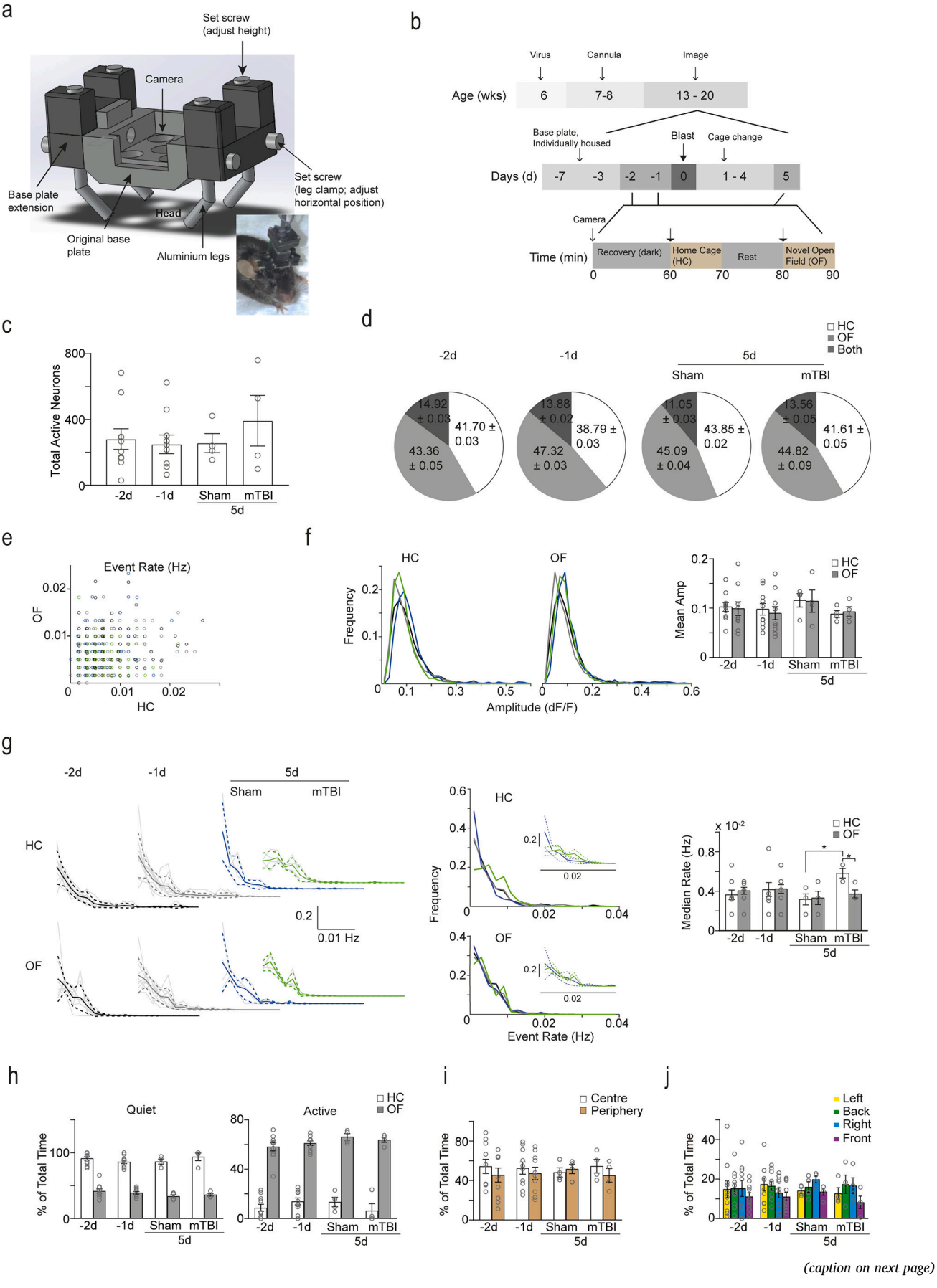

(caption on next page)

Fig. 1. a. Modified base plate design enabling better focus. Inset: Imaging setup. b. Experimental timeline. Closed arrows in row 3 indicate the start of imaging in the environment. Animals in their HCs were placed in the imaging enclosure twice for 10 min on the day of injury (d0) and on 1d, after which cages were changed. c. Total number of active neurons in both environments on each day. All group sizes: $n = 10$ animals (-2d & -1d) & $n = 4$ animals each (sham & mTBI). Data from two casualties of blast was retained in the pre−injury groups. All bar graphs: grey open circles represent individual animals and data is presented as mean ± sem. d. Fraction of neurons active in each environment on the different days. Data is mean ± sem. e. Event rates of individual neurons active in both environments from all animals. Colors for each group (black: −2d, grey: −1d, blue: sham, green: mTBI) are preserved throughout. f. Average frequency histograms of event amplitudes (solid lines from Supplementary Fig. 3c), and bar graph showing mean amplitudes. g. Frequency histograms of calcium event rates. Left: Histograms in both environments on the imaging days. Light grey lines represent histograms of individual animals. Solid and dashed colored lines represent the average and standard deviation of the individual animal histograms in each group. Middle: Average histograms (solid lines in left panels) in the HC (standard deviations of sham and mTBI are shown in the inset figure) and OF. Right: Bar graph showing distribution medians. * $p = 0.0286$ for both, Mann-Whitney test. Some animals had similar median event rates that overlap in the plot. h, i, j Fraction of time animals were (h) quiet and active in the 2 environments, (i) in the center and periphery of the OF, and (j) explored each wall of the OF. (For interpretation of the references to colour in this figure legend, the reader is referred to the web version of this article.)

Given our previous finding of reduced excitability in CA1 after blast mTBI (Beamer et al., 2016), we first asked if there was a decrease in amplitudes of the calcium transients (Fig. 1f, Supplementary Fig. 3c). Mean amplitudes in the injured group were slightly smaller than those in sham but not significantly different ($p > 0.200$ for both HC and OF, Mann-Whitney test). Next, we focused on the temporal dynamics of CA1 neurons in the two environments. Parsing the fraction of cells active in each recorded minute in both environments (Supplementary Fig. 3d), we observed that a larger number were active initially in the first minute or two of recording after which the fraction stabilized, and that the trend persisted after mTBI. Event rates in the familiar HC and novel OF were distributed similarly across both pre-injury days and on 5d in the sham group, emphasizing the stability of the responses (Fig. 1g). We asked how CA1 activity differs in a familiar environment that is not the HC but one that the animal is exposed to briefly such as the same OF (Supplementary Fig. 4). To this end, we compared the event rates of sham (essentially naïve in our injury model) mice in the HC with those of naïve mice in a familiar OF on equivalent days (Supplementary Fig. 4). Median pre-injury and 5d sham event rates in the HC were slightly but not significantly smaller than those in naïve mice in a familiar OF on equivalent days (Supplementary Fig. 4), suggesting that activity in the HC in a familiar context on 5d may be a measure of basal hippocampal activity. Unexpectedly, mTBI did not alter activity in the novel OF (Fig. 1g). More surprisingly and most strikingly, we found that mTBI significantly increased the median activity of neurons in the HC (Fig. 1g) compared with those in the OF and sham HC ($p = 0.028$ for both, Mann-Whitney test; $p = 0.037$, Friedman's one-way repeated measures ANOVA).

We then asked if the increased neuronal activity in the HC was due to an increase in the animals' behavioral activity. Behavior was automatically classified into active and quiet intervals (see methods, Supplementary Fig. 1). Mice were mostly quiet in their HC on all days (Fig. 1h). Interestingly, we found that this behavior was more pronounced in the injured mice; 3 out 4 of which were quiet for the entire duration of the HC recording. In stark contrast, we found that mice were very active in the novel OF on all the days (Fig. 1h), constantly moving throughout the field (Fig. 1i) and examining all four novel walls by leaning and sniffing (Fig. 1j). Together, these results indicate that while the ability of CA1 to detect contextual novelty is unimpaired, its basal state is altered after mTBI. Finally, we asked if the observed changes in neuronal activity after mTBI altered the dimensionality of the population i.e., the number of network states (Carrillo-Reid et al., 2017). There was no change in the dimensionality in either the HC or OF (Supplementary Fig. 3e, f).

In summary, our results show that concussion increases CA1 activity during prolonged awake immobility in the familiar HC. The differences in the responses in the two environments suggests that the CA1 circuitry comparing the incoming entorhinal cortex and Schaffer collateral inputs to detect novelty may not be impaired but that the basal state Schaffer collateral inputs are modified after mTBI. We speculate that this finding is the result of increased excitation of the CA3 recurrent system due either to decreased subcortical modulation or failure of the local hippocampal mechanisms normally suppressing recurrent excitation after injury (Buzsáki, 2015). The explanation, if accurate, predicts an increase in the frequency of sharp wave ripples (SWRs) in CA1 during prolonged awake immobility in the HC, providing a locus for commonly reported memory impairments after concussion (Buzsáki, 2015; Zhou et al., 2019). More broadly, our findings have major implications for post-concussion treatment in the military and civilian population. Cognitive rest, part of the clinical guidelines for treatment, is prescribed to reduce the metabolic load associated with neural processing and thereby accelerate recovery (Barkhoudarian et al., 2016). Intriguingly, some clinical studies show that cognitive rest does not impact recovery time but on the contrary prolonged cognitive rest exacerbates symptoms and delays their resolution (McLeod et al., 2017). As awake, immobile animals share many features of cognitive rest treatment in humans, our results imply that prolonged rest for the recovering brain may increase the metabolic burden on the brain, and raise the need for extensive work examining post-concussion metabolism during different brain states. As concussion can affect the fundamental processes of memory, mood and sleep simultaneously, it is hoped that these results will enable effective treatment for mTBI.

Methods

All experiments were performed on male C57BL6 mice (Charles River Laboratories) in accordance with the guidelines of the Institutional Animal Care and Use Committee (IACUC) of the University of Pennsylvania. For all survival procedures requiring anesthesia, anesthesia was induced with 3% isoflurane mixed with oxygen (100%, Air Gas, PA) and maintained with 1–2% of the same (the percentage of isoflurane was lowered to 2% immediately after the animal was under and subsequently lowered in decrements of 0.5% as the duration under increased). Depth of anesthesia was frequently gauged by the paw pinch test and the percentage of isoflurane was increased to a maximum of 2% if a reflex was observed. Animals were placed on a regulated heating pad throughout the surgical procedures and their eyes were lubricated to prevent corneal damage under anesthesia. They were housed under the standard normal 12 h/12 h dark-light cycle and their weight and general health were monitored once a week throughout the study.

Virus Injection

AAV9.CamKII.GCaMP6f.WPRE.SV40 and AAV9.Syn.GCaMP6f.WPRE.SV40 were obtained from the Penn Vector Core. Mice were unilaterally injected in either their right ($n = 10$) or left ($n = 9$) dorsal CA1 (RC: 1.8–2.0 mm from bregma, ML: 1.4–1.6 mm from midline and DV: 1.3–1.4 mm from the surface of the brain) with 1 µl of either Syn.GCaMP6f ($4.75e^{12}$ GC ml^{-1}, $n = 3$; $2.37e^{12}$ GC ml^{-1}, n = 1 was used only for behavior control) or CamKII.GCaMP6f ($1.14e^{13}$ GC ml^{-1}, $n = 8$; $1.14e^{12}$ GC ml^{-1}, $n = 7$). After induction of anesthesia, animals were placed on a stereotaxic frame (Stoelting Co., IL) and their heads fixed. The skin on their heads was cleaned with povidone-iodine solution (10%, Betadine® Solution) and isopropyl alcohol (70%) after which an incision was made in the middle.

Bupivacaine hydrochloride (2 mg kg^{-1}) was injected into the periosteum and the latter cleared with a cotton swab. Hydrogen peroxide (3%) was lightly dabbed on the sutures to better expose them. A small hole was carefully drilled with a burr (0.5 mm tip diameter, Fine Science Tools Inc., CA) and the needle (26 s/2″/2, Hamilton Company, NV) was positioned at the aforementioned coordinates. The tissue was allowed to settle for 2 min before starting infusion (0.125 μl min^{-1}, Stoelting Co.). Two minutes after completion of infusion, the needle was slowly retracted over the course of 5–10 min and the skin sutured (5–0 dissolvable sutures, EMSCO Scientific Enterprises Inc., PA). Meloxicam (5 mg kg^{-1}) was administered subcutaneously at the nape prior to the start of the procedure and one day after injection.

Preparation of hippocampal window

One (n = 17) or two (n = 2) weeks after virus injection a stainless steel (1.3 mm inner diameter, HTX−15R, Component Supply, TN) cannula sealed with a glass cover slip (0.13–0.17 mm, Fisher Scientific, MA) at one end was inserted above the hippocampus as follows. Animals were first head fixed, their skulls exposed and cleared of overlying tissue as above. The skull was then thoroughly cleaned with hydrogen peroxide (30%, Sigma Aldrich) and the skin glued (Vetbond ™/MC, No. 1469 SB) along the circumference. A circular aperture centered at the injection site was slowly drilled into the skull with a trephine (1.8 mm tip diameter, Fine Science Tools Inc.) and the brain exposed. The dura was removed, and the neocortex and external capsule were continuously flushed with sterile saline and gently aspirated as described (Dombeck et al., 2010) to expose the underlying hippocampus. Bleeding was stemmed with Gelfoam® (Midwest Veterinary Supply, MN), subsequent to which the cannula was gently inserted into the saline filled aspirated cavity. Once positioned in place, Kwik-Sil™ (WPI, FL) was applied around it to hold it in place. Dental cement was then applied uniformly on the entire exposed skull to secure the cannula and provide a scaffold for the baseplate of a miniature microscope (iNSCOPIX, CA). Meloxicam (5 mg kg^{-1}) was administered subcutaneously at the nape prior to the start and for two days after the procedure.

Baseplates were cemented at least one, but typically four, days prior to the commencement of the study. The original camera base plate was customized to move both vertically and horizontally to ensure that the cells were always in focus (Fig. 1a). Briefly, animals were placed on a sterotax under anasesthesia and their cannulas cleaned with distilled water. A GRIN lens, (1.0 mm diameter, iNSCOPIX) that serves as the relay lens between the glass cover slip of the cannula and the miniature microscope, was then inserted into the cannula. The lens was secured to the cannula to prevent displacement during imaging with silicone grease applied very lightly around its circumference halfway through its length. The baseplate was centered so that the complete field of view of the GRIN lens was visible through the camera and the assembly was then cemented to the cement scaffold with additional dental cement. Upon conclusion of the study, animals were deeply anaesthetized with pentobarbital (100 mg kg^{-1}) and perfused with 4% paraformaldehyde. The brains were removed, and the location of the imaging window was confirmed.

Primary blast injury

To enable the collection of pre and post injury data in the same animal, mTBI was caused by blast overpressure to the head as described previously (Beamer et al., 2016). Briefly, animals were first deeply anaesthetized with isoflurane (3% for induction for 5 min and 2% for maintenance for 3 min) and then placed on a holder outside the exit end of a shock-tube with their snouts facing the tube. Their torsos and extremities were protected from the shockwave by sorbothane-lined aluminum casing and their heads constrained from moving with a thin metal rod encircling the snout and a cervical collar positioned between the occiput and shoulders. A subset of animals (n = 8; mTBI group) were then exposed to a mild blast peak incident overpressure of 215 ± 13 kPa, duration of 0.65 ± 0.04 ms, and an impulse of 46 ± 5 kPa*msec. A subset of animals (n = 7; sham group) were not exposed to the blast and served as procedural controls. Mice were randomly assigned into blast and sham groups. After blast or sham exposure, the righting time was used to assess severity of injury. Mice took 143.84 ± 120.41 (mean ± std) s to right after injury and 85.22 ± 92.40 s after sham procedures. Blast did not displace or damage the imaging preparation unless the cement scaffold securing the cannula was insufficiently adhered to the skull, in which case it dislodged the intact preparation from the brain. In the latter event, animals were euthanized immediately.

Imaging

Activity of CA1 neurons was imaged over the course of two weeks starting at least 7 weeks after virus injection when the animals were between 13 and 20 weeks old. Animals were handled once a week for 1–2 min in the interim and on the day before the first imaging session. On each imaging day, animals were briefly (6.70 ± 3.81 min, mean ± std) anaesthetized and the miniscope was mounted onto its baseplate. Upon completion of imaging, the miniscope was usually removed by constraining the mouse briefly with one hand. Anesthesia was only induced if the animal was difficult to constrain making the maneuver difficult.

Animals were transferred to their own separate cages (referred to as home cage in this manuscript) at least one day prior to the start of the imaging study but typically on the day the base plate was attached and were housed individually for the two-week duration. Cages were changed once a week and cage changes were avoided in the middle of the block of consecutive imaging days (first change was performed on the first day after injury). Images, on all the days of study, were acquired during the day in a small enclosure near a corner of a dark room (Supplementary Fig. 1a) under red light. The time of the day at which the activity of any given animal was imaged was kept approximately the same (within 25 min of the start time on the first day of imaging) for the animal throughout the study. After mounting the camera and adjusting the focus, animals were allowed to recover from anesthesia in their home cage (HC) for at least an hour (proportionally more if the duration under anesthesia was a little longer than usual) on a table perpendicular to the imaging enclosure (see Supplementary Fig. 1a). Activity was imaged in two environments for ten minutes each. First in the animal's HC and then in a 'novel' open field (45.1 × 45.1 × 17.6 cm polycarbonate arena) with ten minutes of rest in between each, during which it was replaced in its HC on the recovery table. To maintain animals' familiarity with the imaging enclosure and procedures on 5d, animals were placed in their HCs in the enclosure twice on the day of (day 0; prior to and after injury) and 1d after injury (separated by 30 min), for the same duration as on the imaged days. Calcium transients were captured at a rate of 20 frames s^{-1}. The LED illumination power and gain for a given animal were kept constant on all the days it was imaged. The LED illumination power for each animal was determined on the first day as the minimum power that clearly showed individual cells and the gain was set at one for all animals. Behavior was simultaneously captured at a rate of ~8 frames s^{-1} with a webcam controlled by user-defined MATLAB® scripts. The rate of acquisition of behavior data (~ 8 frames s^{-1}) was constrained such that the least number of frames were dropped by the iNSCOPIX acquisition software. The acquired data was subsequently processed in MATLAB®.

Novelty in the open field

Novelty in the open field (OF) arena on each of the imaging days was provided by completely covering its walls with materials of different textures and with different pictures (see Supplementary Fig. 1b). Textures ranged from that of the bare polycarbonate of the arena to reusable coarse domestic shelf liners and file enclosures containing pictures to disposable brown paper of grocery bags, crinkly tissue paper and the smooth and highly reflective printer paper. Pictures varied from simple shapes such as a circle or triangle to a more complex pattern of

squares or tiles to natural scenes such as grass. The reusable textures viz., shelf liners and file holders were doused with ethanol and cleaned between animals on the same day and at the end of the day they were washed with soap water. The disposable paper textures were replaced with new ones for each animal. The arena was thoroughly wiped with water and ethanol, and the floor was covered with a fresh piece of laboratory shelf liner before placing an animal. The floor on each of the days was randomly arranged with chocolate shavings. Animals were given their first taste of a small shaving of chocolate on the day that they were transferred to their own cage. Animals ($n = 5$) prepared for but excluded from calcium imaging due to the absence of visible cells were used to control for behavior in the absence of chocolate shavings (Supplementary Fig. 1e).

Analysis of behavior

The animal's image in each frame of the behavior sequence was automatically segmented and its centroid determined as described previously (Patel et al., 2014). Due to movement of the miniscope wire and the dim red lights, centroids were frequently off the animal's image and were corrected manually in those frames. The image centroids in each frame were used to mark the animal's position in the environment in all subsequent analysis. Behavior in both environments was automatically divided into two intervals of 'active' and 'quiet' based on empirical displacement of the centroid (Supplementary Fig. 1c). These intervals were subsequently manually checked by an investigator blind to the treatment group. In the manual classification, active intervals included the larger displacements of ambulation, leaning, rearing and smaller displacements of turns and limb extensions. Quiet intervals excluded all movements except for small head movements and centroid jitter. The automatic classifier overestimated quiet times by approximately 5% in the HC and 16% in the OF (Supplementary Fig. 1d). Results from the automatic classifier are reported here. For the standard OF measures of time spent in center and periphery, the periphery was set at 11% of the total area i.e., approximately 5 cm from each wall.

Analysis of calcium transients or events

The acquired time-series in the two environments on each day were processed individually. Images in a series were registered to correct for horizontal or in-plane motion and normalized by the mean intensity image after subtraction of the same (background subtraction, $\frac{dF}{F} = \frac{fij - Fi}{Fi} f_{ij}$ is the intensity in pixel i in frame j and F_i is the mean intensity in pixel i over time). Regions of Interest (ROI) and the transients therein were first automatically extracted from the raw motion corrected time-series using constrained non-matrix factorization (CNMF-E) (Zhou et al., 2018). To ascertain that the ROI corresponded with a neuron and that the calcium transients were true calcium events in the neuron and not the result of bleed through fluorescence from adjacent overlapping cells or local neuropil fluorescence, each ROI and transient associated with it was then manually inspected in the background subtracted time-series (Supplementary Fig. 2) as follows. First, maximum intensity projections and waveforms of the ROI from the background subtracted time-series in its entirety were examined and all ROI that did not obviously correspond with cells were discarded. Second, local maximum intensity images of all transients (i.e., maximum intensity within the frames comprising FWHM of a transient) with amplitudes greater than 10 in the CNMF-E waveform of a retained ROI were generated from the background subtracted time-series and all transients that were contained within the ROI with amplitudes larger than 3 standard deviations of the dF/F waveform were retained. The dF/F waveforms were then cleaned by setting all points except those of the retained transients to zero. These waveforms were used for all subsequent analysis.

ROI common to both time-series on each day were identified as follows. ROI from both time-series with centroids within 3x3μm square neighborhood and distance less than 4.5 μm of each other were first identified. The boundaries of these were then overlaid on the maximum intensity projection images of the two series and their correspondence manually verified. All pairs that did not enclose cells in both images were discarded.

Event rate was calculated as the number of above threshold transients (events) in the entire duration of recording. Transients that started prior to the start of the recording and decayed after the recording was stopped were excluded. Event rates were found to be below 0.035 Hz in accordance with published estimates (Zhou et al., 2019) and were similarly distributed between neurons transfected with GCamp6f under the CamKII and Synapsin promoters (Supplementary Fig. 3a). Population rate vectors with a bin size of one-minute were constructed from z-scored number of transients that started within the one-minute intervals. The eigenvalues of their covariance matrices were determined, and the population vectors were projected onto the first two eigenvectors or principal components to observe the number of network states or dimensionality of the population (Carrillo-Reid et al., 2017). Data analysis was performed by an investigator blind to the treatment group.

Statistics

Data was plotted in MATLAB® or GraphPad (San Diego, CA) and the final figures assembled in Adobe Illustrator®. Non-parametric statistics were used for desired comparisons (GraphPad). Comparisons were made with each animal treated as an independent sample. A p-value of less than 0.05 was considered significant. Group sizes were finalized based on the statistical significance of the results.

Supplementary data to this article can be found online at https://doi.org/10.1016/j.expneurol.2020.113435.

Author contributions

data acquisition (SRT, MAH), data analysis (SRT), manual behavior analysis (AN), experimental design and manuscript preparation (SRT, DFM).

Declaration of Competing Interest

None for all the authors.

Acknowledgements

The authors thank Drs. Mikhail Y Lipin, Brian N Johnson, and Guoxiang Xiong for their invaluable technical assistance, Konrad Körding for suggestions on the data and Bonnie Firestein for comments on the manuscript. Funding was provided by the Paul G. Allen Frontiers group grant #12347 and NIH NS 088176.

References

Atkins, C.M., 2011. Decoding hippocampal signaling deficits after traumatic brain injury. Transl. Stroke Res. https://doi.org/10.1007/s12975-011-0123-z.

Barkhoudarian, G., Hovda, D.A., Giza, C.C., 2016. The molecular pathophysiology of concussive brain injury – an update. Phys. Med. Rehabil. Clin. N. Am. 27, 373–393. https://doi.org/10.1016/j.pmr.2016.01.003.

Beamer, M., Tummala, S.R., Gullotti, D., Kopil, K., Gorka, S., Abel, Ted, Bass, C.R.D., Morrison, B., Cohen, A.S., Meaney, D.F., 2016. Primary blast injury causes cognitive impairments and hippocampal circuit alterations. Exp. Neurol. 283, 16–28. https://doi.org/10.1016/j.expneurol.2016.05.025.

Buzsáki, G., 2015. Hippocampal sharp wave-ripple: a cognitive biomarker for episodic memory and planning. Hippocampus 25, 1073–1188. https://doi.org/10.1002/hipo.22488.

Carrillo-Reid, L., Yang, W., Kang Miller, J., Peterka, D.S., Yuste, R., 2017. Imaging and optically manipulating neuronal ensembles. Annu. Rev. Biophys. 46, 271–293. https://doi.org/10.1146/annurev-biophys-070816-033647.

Chen, Y.H., Kuo, T.T., Huang, E.Y.K., Hoffer, B.J., Chou, Y.C., Chiang, Y.H., Ma, H.I., Miller, J.P., 2018. Profound deficits in hippocampal synaptic plasticity after traumatic brain injury and seizure is ameliorated by prophylactic levetiracetam. Oncotarget 9, 11515–11527. https://doi.org/10.18632/oncotarget.23923.

Dombeck, D.A., Harvey, C.D., Tian, L., Looger, L.L., Tank, D.W., 2010. Functional imaging of hippocampal place cells at cellular resolution during virtual navigation. Nat. Neurosci. 13, 1433–1440. https://doi.org/10.1038/nn.2648.

Johnson, B.N., Palmer, C.P., Bourgeois, E.B., Elkind, J.A., Putnam, B.J., Cohen, A.S., 2014. Augmented inhibition from cannabinoid-sensitive interneurons diminishes CA1 output after traumatic brain injury. Front. Cell. Neurosci. 8. https://doi.org/10.3389/fncel.2014.00435.

Lisman, J., Otmakhova, N., 2001. Storage, recall, and novelty detection of sequences by the hippocampus: {…}. Hippocampus 568, 551–568.

McLeod, T.C.V., Lewis, J.H., Whelihan, K., Bacon, C.E.W., 2017. Rest and return to activity after sport-related concussion: a systematic review of the literature. J. Athl. Train. 52, 262–287. https://doi.org/10.4085/1052-6050-51.6.06.

Meaney, D.F., Morrison, B., Bass, C.D., 2014. The mechanics of traumatic brain injury: a review of what we know and what we need to know for reducing its societal burden. J. Biomech. Eng. https://doi.org/10.1115/1.4026364.

Patel, T.P., Gullotti, D.M., Hernandez, P., O'Brien, W.T., Capehart, B.P., Morrison, B., Bass, C., Eberwine, J.E., Abel, T., Meaney, D.F., 2014. An open-source toolbox for automated phenotyping of mice in behavioral tasks. Front. Behav. Neurosci. 8. https://doi.org/10.3389/fnbeh.2014.00349.

Paterno, R., Folweiler, K.A., Cohen, A.S., 2017. Pathophysiology and treatment of memory dysfunction after traumatic brain injury. Curr. Neurol. Neurosci. Rep. https://doi.org/10.1007/s11910-017-0762-x.

Witgen, B.M., Lifshitz, J., Smith, M.L., Schwarzbach, E., Liang, S.L., Grady, M.S., Cohen, A.S., 2005. Regional hippocampal alteration associated with cognitive deficit following experimental brain injury: a systems, network and cellular evaluation. Neuroscience 133, 1–15. https://doi.org/10.1016/j.neuroscience.2005.01.052.

Zhou, P., Resendez, S.L., Rodriguez-Romaguera, J., Jimenez, J.C., Neufeld, S.Q., Giovannucci, A., Friedrich, J., Pnevmatikakis, E.A., Stuber, G.D., Hen, R., Kheirbek, M.A., Sabatini, B.L., Kass, R.E., Paninski, L., 2018. Efficient and accurate extraction of in vivo calcium signals from microendoscopic video data. eLife 7. https://doi.org/10.7554/eLife.28728.

Zhou, H., Neville, K.R., Goldstein, N., Kabu, S., Kausar, N., Ye, R., Nguyen, T.T., Gelwan, N., Hyman, B.T., Gomperts, S.N., 2019. Cholinergic modulation of hippocampal calcium activity across the sleep-wake cycle. eLife 8. https://doi.org/10.7554/eLife.39777.